ELSEVIER

Journal of Fluids and Structures 23 (2007) 1251–1264

JOURNAL OF FLUIDS AND STRUCTURES

www.elsevier.com/locate/jfs

Aerothermoelastic behavior of supersonic rotating thin-walled beams made of functionally graded materials

S.A. Fazelzadeh*, M. Hosseini

Department of Mechanical Engineering, School of Engineering, Shiraz University, Shiraz 71344, I.R. Iran

Received 28 April 2006; accepted 17 June 2007

Abstract

In this study, a thin-walled beam made of functionally graded material (FGM) which is used as rotating blades in turbomachinery under aerothermoelastic loading is investigated. The governing equations, which are based on first-order shear deformation theory, include the effects of the presetting angle, the secondary warping, temperature gradient through the wall thickness of the beam and also the rotational speed. Moreover, quasi-steady aerodynamic pressure loadings are determined using first-order piston theory, and steady beam surface temperature is obtained from gas dynamics theory. Then, the blade partial differential equations are transformed into a set of ordinary differential equations using the extended Galerkin method. Finally, having solved the resulting structural–fluid–thermal eigenvalue system of equations, the effects of Mach number and geometric parameters on natural frequencies are presented. The results demonstrate that the natural frequencies decrease under aerothermoelastic loading at high Mach numbers.

Keywords: Aerothermoelasticity; Functionally graded materials; Supersonic flow; Rotating blade; High-temperature field

1. Introduction

Rotating blades in turbomachinery operate at high speed and temperature. Due to aerothermoelastic interactions especially at high Mach number, rotating blades are subjected to high aerothermal loads which can cause instability behavior during operation, as pointed out by Oh et al. (2003a, b). Librescu (1975) showed that static and dynamic instabilities are induced by high speed airflow and greatly affected by the thermal environment. Functionally graded materials (FGMs) for high-temperature structural applications are special microscopically inhomogeneous composites, whose thermo-mechanical properties vary smoothly and continuously in predetermined directions throughout the body of the structure. This feature is achieved by gradually varying the volume fraction of constituent materials, which usually are ceramics and metals (Aboudi et al., 1966). The limitations of such a homogenization-based approach in the analysis of FGMs have been discussed by Pindera et al. (1995). In addition to the research works for the modeling of three-dimensional (3-D) FGM media (such as Aboudi et al., 1999; Librescu et al., 2005; Oh et al., 2003a, b), the studies involving thin-walled structures made of FGMs have also been devoted to beams, plates, and shells (Sanker, 2002). Librescu et al. (2005) studied the rotating FGM thin-walled beams operating in a high-temperature environment, without the gas flow pressure loading. To the best of the authors' knowledge, in spite of its evident practical importance,

*Corresponding author. Tel.: +98 711 2303051; fax: +98 711 6287294.
E-mail address: Fazelzad@shirazu.ac.ir (S.A. Fazelzadeh).

0889-9746/$ - see front matter
doi:10.1016/j.jfluidstructs.2007.06.006

Nomenclature

a	blade width
a_{ij}	stiffness quantities
a_x, a_y, a_z	acceleration components of arbitrary point on beam cross-section
$[A]$	state matrix
b	blade height
b_k	mass quantities
$C_{\beta\gamma}$, $S_{\beta\gamma}$	direction cosines between principal and blade coordinate directions
C_∞	sound speed
E	Young's modulus
$[G]$	aerodynamic damping matrix
h	wall thickness
k	volume fraction parameter
$[K]$	stiffness matrix
L	blade length
m_x, m_y	distributed moment
M_x, M_y	the moments about the x- and y-axis
M_x^T, M_y^T	thermal moment about x- and y-axis
$[M]$	mass matrix
M_∞	Mach number
N	number of mode
p_x, p_y	distributed force in x- and y-direction
p_{nx}, p_{ny}	x and y of non-aerodynamic loading
$\{q_u\}$, $\{q_v\}$, $\{q_x\}$, $\{q_y\}$,	generalized coordinates
$\{Q\}$	forcing vector
Q_x, Q_y	the shear forces in the x- and y-directions
$\{R\}$	position vector of an arbitrary point of the blade
R_f	steady temperature recovery factor
R_0	hub radius
s, n	local surface coordinates (tangential, normal to mid-surface)
T_∞	air flow temperature
T_z	the axial force in the z-direction
u, v, w	displacement components in the x-, y- and z-direction
u_0, v_0	displacement components in the x- and y-direction
$\{U\}$, $\{V\}$	N-dimensional vectors of trial functions of displacement
U_0, V_0	amplitude of displacement components in the x- and y-direction
$U_{x^p}^t$, $U_{y^p}^t$	the tangential components of fluid velocity on the positive x^p and y^p planes
U_∞	air flow velocity
v_x, v_y, v_z	velocity components of arbitrary point on beam cross-section
V_m, V_c	volume fraction of metal and ceramic
x, y, z	blade coordinate variables
x^p, y^p, z^p	principal coordinate variables
$\{X\}$	constant vector
$\{Z\}$	state vector
α	thermal expansion coefficient
β, β_0	pretwist angle of an arbitrary cross-section and tip cross-section, respectively
δT, δV, δW_e	variation of kinetic and potential energy and virtual work of external force, respectively
Δp_{x^p}, Δp_{y^p}	the x- and y-aerodynamic loading on the positive x^p and y^p planes
ΔT	the steady-state temperature rise
ε_{xx}, ε_{yy}	in-plane strain
γ	setting angle
γ_{xy}	in-plane shear strain
γ_{yz}, γ_{xz}	transverse shear strain
θ_x, θ_y	rotation about x- and y-axis, respectively
$\{\Theta_x\}$, $\{\Theta_y\}$	N-dimensional trial vectors of rotation about x- and y-axis, respectively
κ	thermal conductivity
κ_a	air polytropic ratio
λ	aerothermoelastic eigenvalue
ν	Poisson's ratio
ρ	material mass density
ρ_∞	air flow density
υ	the lateral velocity of gas particles near the panel surface
σ_{ij}	the stress tensor components
ω_i	natural frequency
$\bar{\omega}_i$	nondimensional natural frequency $(\omega_i L^2\sqrt{b_1/a_{33}})$
Ω	rotating speed
$\bar{\Omega}$	nondimensional angular velocity of the shaft $(\Omega L^2\sqrt{b_1/a_{33}})$
$(\dot{.}), (.)'$	$(\mathrm{d}/\mathrm{d}t)(.)$, $(\mathrm{d}/\mathrm{d}z)(.)$

no research work related to the modeling and aerothermoelastic behavior of supersonic rotating FGM thin-walled beams working under a gas flow pressure as well as in a high-temperature environment has been done yet. Hence, the research work in this paper is devoted to this topic.

A thin-walled beam made of FGM is considered, which is used as a rotating turbomachinery blade under aerothermoelastic loading. The governing equations, based on a small-deflection beam model are considered, including the presetting angle. It is assumed that the original cross-section of the blade is preserved and transverse shear and rotary inertias are included in the structural model. Also the effect of rotational velocity has been taken into account. Quasi-steady aerodynamic pressure loadings are determined using first-order piston theory as well as steady beam surface temperature through gas dynamic theory (Pourtakdoust and Fazelzadeh, 2005). In this investigation the blade is

exposed to viscous compressible flow at a constant speed for a sufficient period of time. From the principle of conservation of energy, it can be concluded that the flow temperature is proportional to the square of Mach number. Finally, the blade partial differential equations are transformed into a set of ordinary differential equations through the extended Galerkin approach. Herein, the damping terms are included in the discretized form of the governing equations of motion, whereas the damping terms do not appear in the absence of gas flow pressure loading (Librescu et al., 2005).

2. Blade geometrical description

Consider a straight and pre-twisted flexible beam of length L mounted on a rigid hub of radius R_0 and spinning at constant speed Ω about an axis normal to the longitudinal axis of the beam, as shown in Fig. 1. The beam is allowed to vibrate flexurally in a plane making an angle γ with respect to the plane of rotation, referred to as the setting angle. In Fig. 1 (x, y, z) is a centroidal (right-hand Cartesian) rotating coordinate system with its origin located at the blade root. In addition to this coordinate system, the principal coordinate system is considered along the principal axes of a beam cross-section (Librescu et al., 2005).

The two coordinate systems are related by the following transformation relationships:

$$x = x^p \cos(\beta(z)+\gamma) - y^p \sin(\beta(z)+\gamma), \quad y = x^p \sin(\beta(z)+\gamma) + y^p \cos(\beta(z)+\gamma), \quad z = z^p, \tag{1}$$

where $\beta(z) = \beta_0 z/L$, is the pre-twist of the given section, β_0 is the pre-twist at the beam tip, and L is the beam span. It should be remarked that (s, z, n) is another local coordinate, where s and n, $-\frac{1}{2}h \leqslant n \leqslant \frac{1}{2}h$, are mid-line circumferential and thickness coordinates, respectively. Here h is the wall blade thickness. Components of the 3-D displacement vector are expressed as

$$\begin{aligned} &u(x,y,z;t) = u_0(z;t), \quad v(x,y,z;t) = v_0(z;t),\\ &w(x,y,z;t) = \theta_x(z;t)\left(y(s) - n\frac{\mathrm{d}x}{\mathrm{d}s}\right) + \theta_y(z;t)\left(x(s) + n\frac{\mathrm{d}y}{\mathrm{d}s}\right), \end{aligned} \tag{2}$$

where u_0 (z;t) and v_0 (z;t) are rigid-body translations along the x- and y-axis, and $\theta_x(z;t)$ and $\theta_y(z;t)$ are rigid-body rotations about the x- and y-axis. The position vector of a point $M(x,y,z)$ belonging to the deformed structure is

$$\{R(x,y,z;t)\} = (x+u)\mathbf{i} + (y+v)\mathbf{j} + (z+w+R_0)\mathbf{k}. \tag{3}$$

By deriving the position vector, one obtains the velocity and acceleration vectors of an arbitrary point $M(x,y,z)$ of the beam in the form

$$\{\dot{R}\} = v_x\mathbf{i} + v_y\mathbf{j} + v_z\mathbf{k}, \quad \{\ddot{R}\} = a_x\mathbf{i} + a_y\mathbf{j} + a_z\mathbf{k}; \tag{4}$$

their components are

$$v_x = \dot{u} + (R_0 + z + w)\Omega, \quad v_y = \dot{v}, \quad v_z = \dot{w} - (x+u)\Omega, \tag{5}$$

$$a_x = \ddot{u} + 2\dot{w}\Omega - (x+u)\Omega^2, \quad a_y = \ddot{v}, \quad a_z = \ddot{w} - 2\dot{u}\Omega - (R_0 + z + w)\Omega^2. \tag{6}$$

The following strain displacement relation can be derived:

$$\varepsilon_{zz} = \frac{\partial w}{\partial z}, \quad \gamma_{xz} = \left(\frac{\partial w}{\partial x} + \frac{\partial u}{\partial z}\right), \quad \gamma_{yz} = \left(\frac{\partial w}{\partial y} + \frac{\partial v}{\partial z}\right). \tag{7}$$

The relation between shear strain in (s, z, n) and (x, y, z) coordinate systems can be obtained as

$$\varepsilon_{sz} = \frac{\mathrm{d}x}{\mathrm{d}s}\gamma_{xz} + \frac{\mathrm{d}y}{\mathrm{d}s}\gamma_{yz}, \quad \varepsilon_{nz} = \frac{\mathrm{d}y}{\mathrm{d}s}\gamma_{xz} - \frac{\mathrm{d}x}{\mathrm{d}s}\gamma_{yz}. \tag{8}$$

It is assumed that the original cross-section of the beam is preserved (Qin and Librescu, 2002), therefore

$$\varepsilon_{xx} = \varepsilon_{yy} = \gamma_{xy} = 0. \tag{9}$$

Consequently, also

$$\varepsilon_{nn} = \varepsilon_{ss} = \varepsilon_{sn} = 0. \tag{10}$$

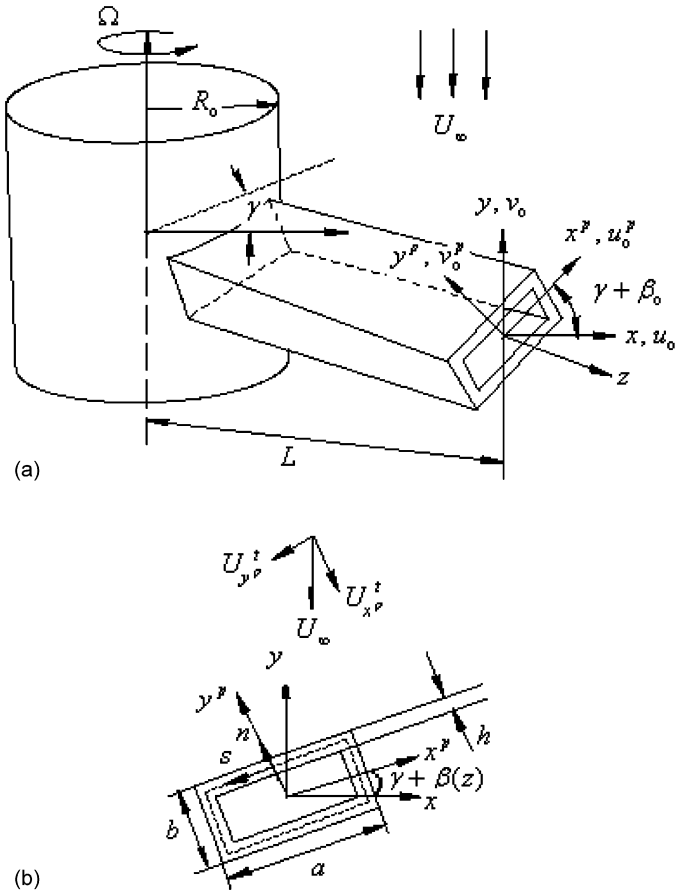

Fig. 1. Geometry of the rotating blades: (a) pretwisted thin-walled blade and (b) blade cross-section.

3. Constitutive relations

Since the material used is isotropic, the corresponding thermoelastic constitutive law adapted to the case of thin-walled structures is expressed as (Noda et al., 2003)

$$\begin{bmatrix}\sigma_{ss}\\ \sigma_{zz}\\ \sigma_{zn}\\ \sigma_{ns}\\ \sigma_{sz}\end{bmatrix}=\begin{bmatrix}Q_{11} & Q_{12} & 0 & 0 & 0\\ Q_{12} & Q_{22} & 0 & 0 & 0\\ 0 & 0 & Q_{44} & 0 & 0\\ 0 & 0 & 0 & Q_{55} & 0\\ 0 & 0 & 0 & 0 & Q_{66}\end{bmatrix}\begin{bmatrix}\varepsilon_{ss}\\ \varepsilon_{zz}\\ \varepsilon_{zn}\\ \varepsilon_{ns}\\ \varepsilon_{sz}\end{bmatrix}-\begin{bmatrix}\hat{\alpha}\Delta T\\ \hat{\alpha}\Delta T\\ 0\\ 0\\ 0\end{bmatrix}, \tag{11}$$

where

$$Q_{11}\frac{E}{1-v^2},\quad Q_{12}=\frac{Ev}{1-v^2},\quad Q_{66}=\frac{E}{2(1+v)},$$
$$Q_{44}=Q_{55}=\kappa_s^2\frac{E}{2(1+v)},\quad \hat{\alpha}=\frac{E}{1-v}\alpha$$

and E and v are Young's modulus and Poisson's ratio, respectively, κ_s^2 is the transverse shear correction factor, $\Delta T(s, z, n)$ is the steady-state temperature rise from that of the stress-free state, and α is the thermal expansion coefficient. The calculation of through-thickness graded properties is based on the assumption that the inclusion phase is small relative to both the wall thickness and temperature gradient. For a model of ceramic/metal FGM the material properties vary

continuously across the blade thickness according to the law given by Praveen and Reddy (1998),

$$PM(n) = (PM_c - PM_m)V_c + PM_m, \quad V_c = 1 - V_m, \tag{12}$$

where V_m and V_c are the volume fractions of metal and ceramic. Herein subscripts m and c identify quantities associated with metal and ceramic, respectively. PM in Eq. (12) represents "material properties" corresponding to the modulus of elasticity, Poisson's ratio, density, thermal coefficient expansion and thermal conductivity.

For the case of an uniform blade thickness, V_m can be expressed as

$$V_c = \left[\frac{2n+h}{2h}\right]^k, \tag{13}$$

where k, $0 \leqslant k \leqslant \infty$, is the volume fraction parameter. This shows that the material properties vary continuously from fully ceramic at the top surface of the blade to fully metal at the bottom surface. It is also assumed that the blade is subjected to a steady-state one-dimensional (1-D) temperature distribution through its thickness. The steady-state 1-D heat transfer equation is expressed by

$$\frac{\mathrm{d}}{\mathrm{d}n}\left[\kappa(n)\frac{\mathrm{d}T}{\mathrm{d}n}\right] = 0. \tag{14}$$

The boundary conditions are

$$T\left(n = -\frac{h}{2}\right) = T_m, \quad T\left(n = \frac{h}{2}\right) = T_c. \tag{15}$$

The solution of Eq. (14) can be obtained by means of polynomial series. Therefore, $T(n)$ is calculated as

$$T(n) = T_m + \frac{\Delta T}{C}\sum_{i=0}^{\infty}(-1)^i \frac{(\kappa_{cm})^i}{(ik+1)(\kappa_m)^i}\left(\frac{2z+h}{2h}\right)^{ik+1} \tag{16}$$

with

$$C = \sum_{j=0}^{\infty}(-1)^j \frac{(\kappa_{cm})^j}{(jk+1)(\kappa_m)^j}$$

and

$$\Delta T = T_c - T_m, \quad \kappa_{cm} = \kappa_c - \kappa_m.$$

Throughout the numerical simulation T_m is taken 300 K. It is assumed that the properties of the FGM are temperature-dependent and vary according to a law obtained experimentally. These are expressed in a general form as

$$P(n) = P_0(P_{-1}/T + 1 + P_1 T + P_2 T^2 + P_3 T^3). \tag{17}$$

Herein P_0, P_{-1}, P_1, P_2, P_3 are constants and T (in degrees Kelvin) is the environmental temperature. For those constituents considered in this paper, namely silicon nitride (SN) and stainless steel (SS), the constants P_i are supplied (e.g., see, Oh et al. (2003a, b) and Reddy and Chin (1998).

4. Governing equation of rotating blades

The governing equations and boundary conditions can be derived via the extended Hamilton's principle. This can be formulated as

$$\int_{t_1}^{t_2}(\delta T - \delta V + \delta W_e)\,\mathrm{d}t = 0, \quad \delta u_0 = \delta v_0 = \delta\theta_x = \delta\theta_x = 0 \text{ at } t = t_1, t_2, \tag{18}$$

where T and V denote the kinetic and strain energies, respectively, δW_e is the virtual work of external forces, t_1 and t_2 being two arbitrary instants of time, and δ is the variational operator. In the above equation, the variation of kinetic energy is given by

$$\delta T = \int_0^L (\rho\{\dot{R}\}\{\delta\dot{R}\})\,\mathrm{d}z, \tag{19}$$

in which

$$\{\dot{R}\} = [\dot{u} + (R_0 + z + w)\Omega]\mathbf{i} + \dot{v}\mathbf{j} + [\dot{w} - (x + u)\Omega]\mathbf{k}.$$

Also, the variation of strain energy based on first-order shear deformation theory of beams can be written as

$$\begin{aligned}\delta V = & -\int_0^L \{(M_y' - Q_x)\delta\theta_y + (M_x' - Q_y)\delta\theta_x + [Q_x' + (T_z u_0')']\,\delta u_0 + [Q_y' + (T_z v_0')']\,\delta v_0\}\,\mathrm{d}z \\ & + [M_y\delta\theta_y + M_x\delta\theta_x + (Q_x + T_z u_0')\,\delta u_0 + (Q_y + T_z v_0')\,\delta v_0]|_0^L,\end{aligned} \tag{20}$$

where (T_z, Q_x, Q_y) and (M_x, M_y) are 1-D stress resultants and couples, respectively. δW_e is the virtual work of nonconservative external forces, which in this study becomes,

$$\delta W_e = \int_0^L (p_x\delta u_0 + p_y\delta v_0)\,\mathrm{d}z. \tag{21}$$

Substituting Eqs. (19)–(21) into Eq. (18), using integration by parts, and noting the fact that the variations (δu_0, δv_0, $\delta\theta_x$, $\delta\theta_y$) are independent and arbitrary, the equations of motion and the related boundary conditions can be obtained as

$$\delta u_0:\ [a_{44}(z)(u_0' + \theta_y) + a_{45}(z)(v_0' + \theta_x)]' - b_1\ddot{u}_0 + b_1 u_0\Omega^2 + \Omega^2[R(z)u_0']' + p_x = 0, \tag{22}$$

$$\delta v_0:\ [a_{55}(z)(v_0' + \theta_x) + a_{54}(z)(u_0' + \theta_y)]' - b_1\ddot{v}_0 + \Omega^2[R(z)v_0']' + p_y = 0, \tag{23}$$

$$\begin{aligned}\delta\theta_y:\ & [a_{22}(z)\theta_y' + a_{23}(z)\theta_x']' - a_{44}(z)(u_0' + \theta_y) - a_{45}(z)(v_0' + \theta_x) - (b_5(z) + b_{15}(z))(\ddot{\theta}_y - \Omega^2\theta_y) \\ & - (b_6(z) - b_{13}(z))(\ddot{\theta}_x - \Omega^2\theta_x) + m_y = (M_y^T)',\end{aligned} \tag{24}$$

$$\begin{aligned}\delta\theta_x:\ & [a_{33}(z)\theta_x' + a_{32}(z)\theta_y']' - a_{55}(z)(v_0' + \theta_x) - a_{54}(z)(u_0' + \theta_y) - (b_4(z) + b_{14}(z))(\ddot{\theta}_x - \Omega^2\theta_x) \\ & - (b_6(z) - b_{13}(z))(\ddot{\theta}_y - \Omega^2\theta_y) + m_x = (M_x^T)',\end{aligned} \tag{25}$$

where M_x^T and M_y^T are thermal bending moments about the x- and y-axis, respectively, and stiffness quantities $a_{ij} = a_{ji}$ and reduced mass terms b_i are defined in Oh et al. (2003a, b) and Librescu et al. (2005). Assuming the blade to be clamped at $z = 0$ and free at $z = L$, the corresponding boundary conditions are:

$$u_0 = v_0 = \theta_y = \theta_x = 0, \text{ at } z = 0, \tag{26}$$

and

$$\delta u_0:\ a_{44}(u_0' + \theta_y) + a_{45}(v_0' + \theta_x) = 0, \quad \delta v_0:\ a_{55}(v_0' + \theta_x) + a_{54}(u_0' + \theta_y) = 0, \tag{27,28}$$

$$\delta\theta_y: a_{22}\theta_y' + a_{23}\theta_x' = M_y^T, \quad \delta\theta_x: a_{33}\theta_x' + a_{32}\theta_y' = M_x^T, \text{ at } z = L. \tag{29,30}$$

5. Aerothermoelastic loadings

It is assumed that the blade is exposed to supersonic gas flow. The temperature difference due to viscous flow can be expressed as

$$\Delta T = T_c - T_\infty = R_f[(\kappa_a - 1)/2]M_\infty^2 T_\infty, \tag{31}$$

where T_c is blade wall temperature. First-order piston theory is used to evaluate the perturbed gas pressure. Hence, the pressure on the principal planes of the blade becomes

$$\Delta P_{y^p} = C_\infty\rho_\infty\left(\frac{\partial v^p}{\partial t} + U_{y^p}^t\frac{\partial v^p}{\partial z}\right), \quad \Delta P_{x^p} = C_\infty\rho_\infty\left(\frac{\partial u^p}{\partial t} + U_{x^p}^t\frac{\partial u^p}{\partial z}\right), \tag{32}$$

where

$$U_{x^p}^t = U_\infty\cos(\beta + \gamma), \quad U_{y^p}^t = U_\infty\sin(\beta + \gamma); \tag{33}$$

here C_∞, ρ_∞, U_∞ are the speed of sound, the free stream air density and velocity, respectively, $U_{x^p}^t$ and $U_{y^p}^t$ are the tangential components of fluid velocity on the positive x^p and y^p planes, respectively. Also, u^p and v^p are displacement

components along the principal axes x^p and y^p, respectively, which are related to the displacement components in the x–y coordinate system as

$$u^p = u_0 \cos(\beta+\gamma) + v_0 \sin(\beta+\gamma), \quad v^p = -u_0 \sin(\beta+\gamma) + v_0 \cos(\beta+\gamma). \tag{34}$$

Using Eq. (32), the external loads per unit axial length distributed in the x- and y-directions can be obtained, respectively, as

$$p_x = a\,\Delta P_{y^p} \sin(\beta+\gamma) - b\,\Delta P_{x^p} \cos(\beta+\gamma), \quad p_y = -a\,\Delta P_{y^p} \cos(\beta+\gamma) - b\,\Delta P_{x^p} \sin(\beta+\gamma). \tag{35}$$

6. Method of solution

Due to the complicated boundary conditions and elastic coupling involved in the governing equations, it is difficult to obtain an exact solution. Therefore, in order to solve the governing equations in a general way, the extended Galerkin's method (EGM) (Reddy, 1986) is used. In this method we must select weighting functions that only need to satisfy boundary conditions. The displacement field is represented as

$$\begin{aligned} &u_0(z,t) = \{U(z)\}^{\mathrm{T}}\{q_u(t)\}, \quad v_0(z,t) = \{V(z)\}^{\mathrm{T}}\{q_v(t)\},\\ &\theta_x(z,t) = \{\Theta_x(z)\}^{\mathrm{T}}\{q_x(t)\}, \quad \theta_y(z,t) = \{\Theta_y(z)\}^{\mathrm{T}}\{q_y(t)\}, \end{aligned} \tag{36}$$

where $\{U\}$, $\{V\}$, $\{\Theta_x\}$ and $\{\Theta_y\}$ are N-dimensional vectors of trial functions. Replacing the displacement field in the governing equations and using EGM, the discretized form of the governing equation of motion for the rotary thin-walled blade is obtained as

$$[M]\{\ddot{q}(t)\} + [G]\{\dot{q}(t)\} + [K]\{q(t)\} = 0, \tag{37}$$

where $[M]$, $[G]$ and $[K]$ denote the symmetric mass matrix, the symmetric aerodynamic damping matrix and the non-symmetric stiffness matrix, respectively, while

$$\{q\} = \left\{\{q_u\}^{\mathrm{T}}\{q_v\}^{\mathrm{T}}\{q_x\}^{\mathrm{T}}\{q_y\}^{\mathrm{T}}\right\}^{\mathrm{T}} \tag{38}$$

is the overall vector of generalized coordinates. The expressions for the $[M]$, $[G]$ and $[K]$ matrices are provided in Appendix A.

Eq. (37) can be expressed in the first-order variable form as

$$\{\dot{Z}(t)\} = [A]\{Z(t)\}, \tag{39}$$

where the state vector $\{Z(t)\}$ is defined as

$$\{Z(t)\} = \{\{q\}^{\mathrm{T}}\{\dot{q}\}^{\mathrm{T}}\}^{\mathrm{T}}, \tag{40}$$

and the $4N \times 4N$ state matrix $[A]$ has the form

$$[A] = \begin{bmatrix} [0] & [I] \\ -[M]^{-1}[K] & -[M]^{-1}[G] \end{bmatrix}, \tag{41}$$

in which $[I]$ is the unit matrix. Upon expressing $\{Z(t)\}$ in Eq. (39) as

$$\{Z(t)\} = \{X\}\exp(\lambda t), \tag{42}$$

a standard eigenvalue problem is obtained,

$$([A] - \lambda[I])\{Z\} = 0, \tag{43}$$

where $\{X\}$ is a constant vector and λ is a constant-valued quantity. The aerothermoelastic eigenvalues or natural frequencies of the structural–fluid–thermal system can be obtained from the resulted equation. In general the eigenvalues are complex (Dowell, 1975).

7. Numerical results

The resulting system of equations is solved through numerical integration. The effects of Mach number variation and geometric parameters on the natural frequencies are presented. The thin-walled blade considered has a uniform

rectangular cross-section with the following geometrical characteristics:

$$R_0 = 1.3\,\text{m}, \quad L = 1.52\,\text{m}, \quad a = 0.257\,\text{m}, \quad b = 0.0827\,\text{m}, \quad h = 0.01654\,\text{m}.$$

The following dimensionless parameters have been considered in the numerical simulations

$$\bar{\Omega}^2 = \Omega^2 \frac{b_1 L^4}{a_{33}}, \quad \bar{\omega}_i^2 = \omega_i^2 \frac{b_1 L^4}{a_{33}},$$

where ω_i is the ith natural frequency of the non-pretwisted and non-rotating blades considered at zero Mach number. The functionally graded material considered is composed of SN and SS with dependent temperature properties given by

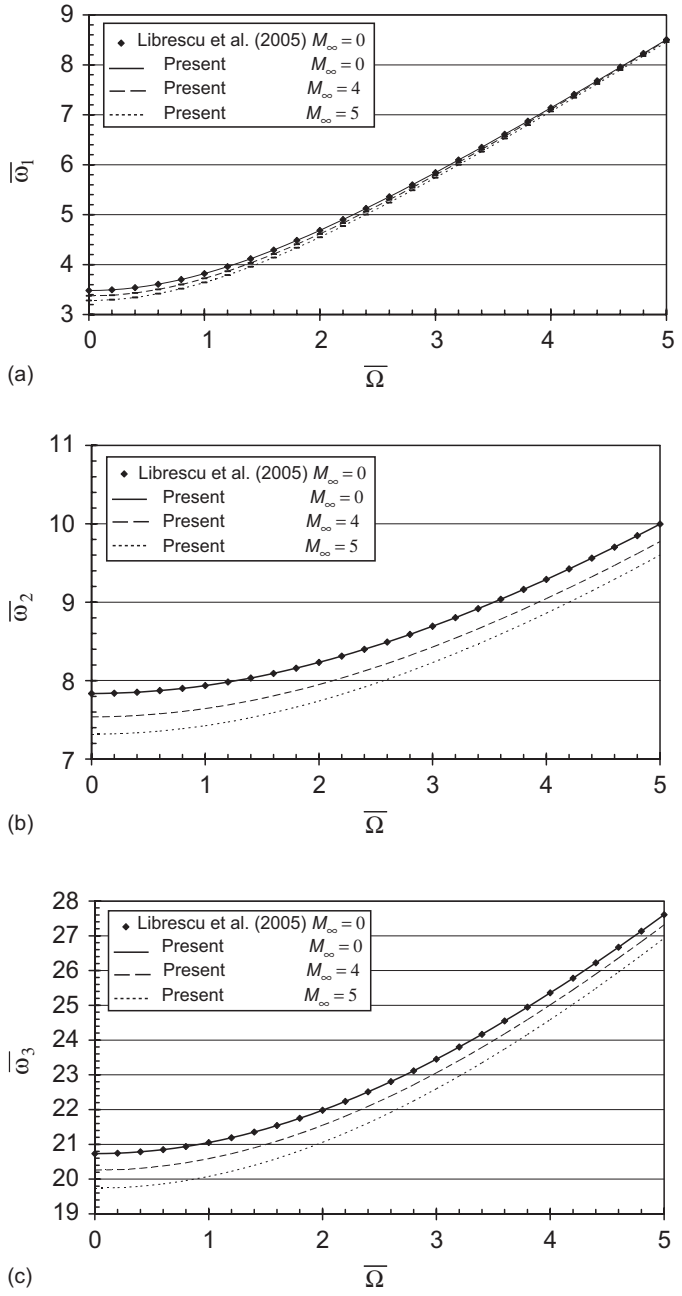

Fig. 2. Variation of the natural frequencies versus rotating speed for selected values of Mach number for $\beta_0 = 45^\circ$, $\gamma = 0$, and $k = 0$.

Oh et al. (2003a, b) and Reddy and Chin (1998).The following properties is considered for air:

$$\kappa = 1.4, \quad T_\infty = 300\,\mathrm{K}, \quad \rho_\infty = 1.1614\,\mathrm{kg/m^3}, \quad C_\infty = 340.5\,\mathrm{m/s}.$$

Trial functions used in EGM are polynomial series satisfying boundary conditions at the root, which are (Chandiramani et al., 2003)

$$\{U\} = \{V\} = \left\{z^2 z^3 z^4 z^5 z^6 z^7\right\}^{\mathrm{T}}, \quad \{\Theta_x\} = \{\Theta_y\} = \left\{z^1 z^2 z^3 z^4 z^5 z^6\right\}^{\mathrm{T}}.$$

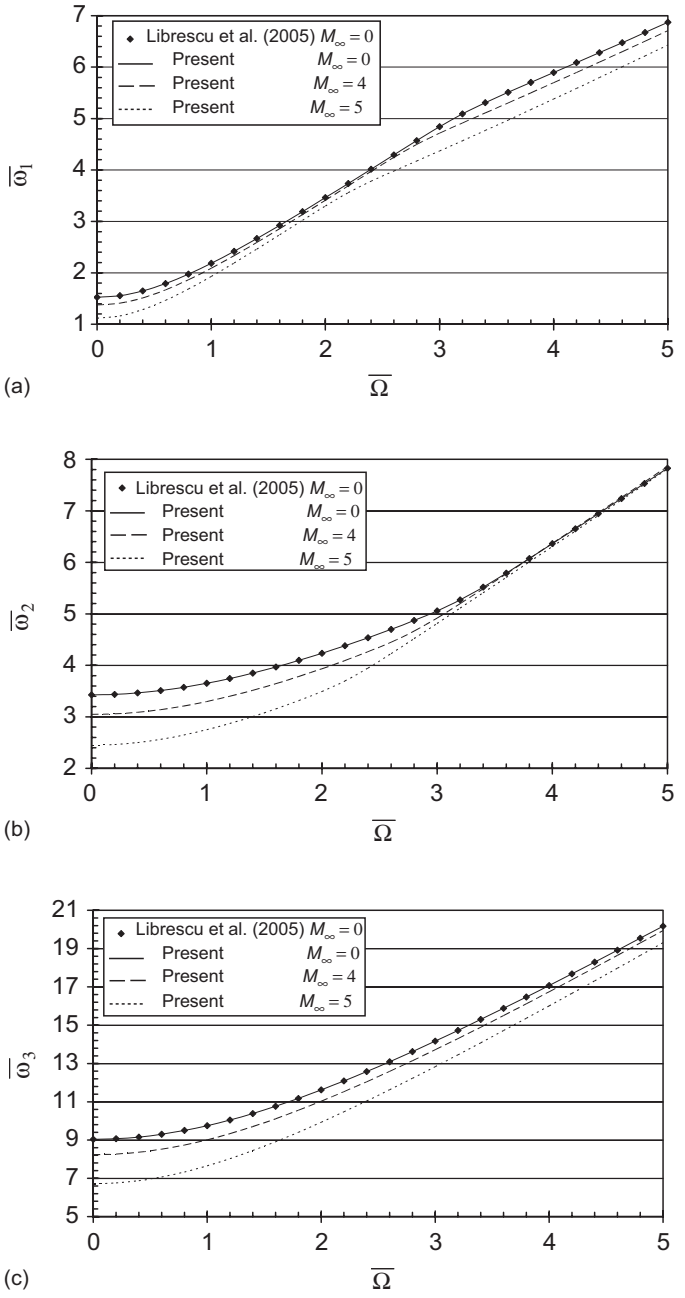

Fig. 3. Variation of the natural frequencies versus rotating speed for selected values of Mach number for $\beta_0 = 45^\circ$, $\gamma = 0$, and $k = 50$.

Also, in Eq. (24) the first six terms of the series are used in the numerical simulations (Lanhe, 2004). In general, the system is nonconservative; therefore, the stiffness matrix $[K]$ is nonsymmetric. For some choices of the displacement components it may become symmetric as in the case of present study, in which we used the same order polynomial spatial basis functions for the displacement components, i.e. $\{U(z)\} = \{V(z)\}$, in the Galerkin solution procedure. The numerical solution yields a result in the form of $\lambda = \sigma + i\omega$, in which σ is of very small magnitude in comparison with ω and therefore $e^{\lambda t} \cong e^{i\omega t}$ At the critical state, $\sigma = 0$, the imaginary part of ω corresponds to the natural frequency or the flutter frequency of the system.

Variation of the first three natural frequencies versus the dimensionless rotating speed for full ceramic material and two Mach numbers are shown in Fig. 2. The results are for zero Mach number compatible with that given by Librescu et al. (2005). It is evident that increasing the Mach number tends to reduce the natural frequency. This is associated with raising the temperature on the wall surface. In contrast to the effect of increasing of the Mach number, the beneficial effect of increasing $\bar{\Omega}$ is observed in this figure. Similar trends appear in the results for the full metal constituent ($k = 50$), plotted in Fig. 3.

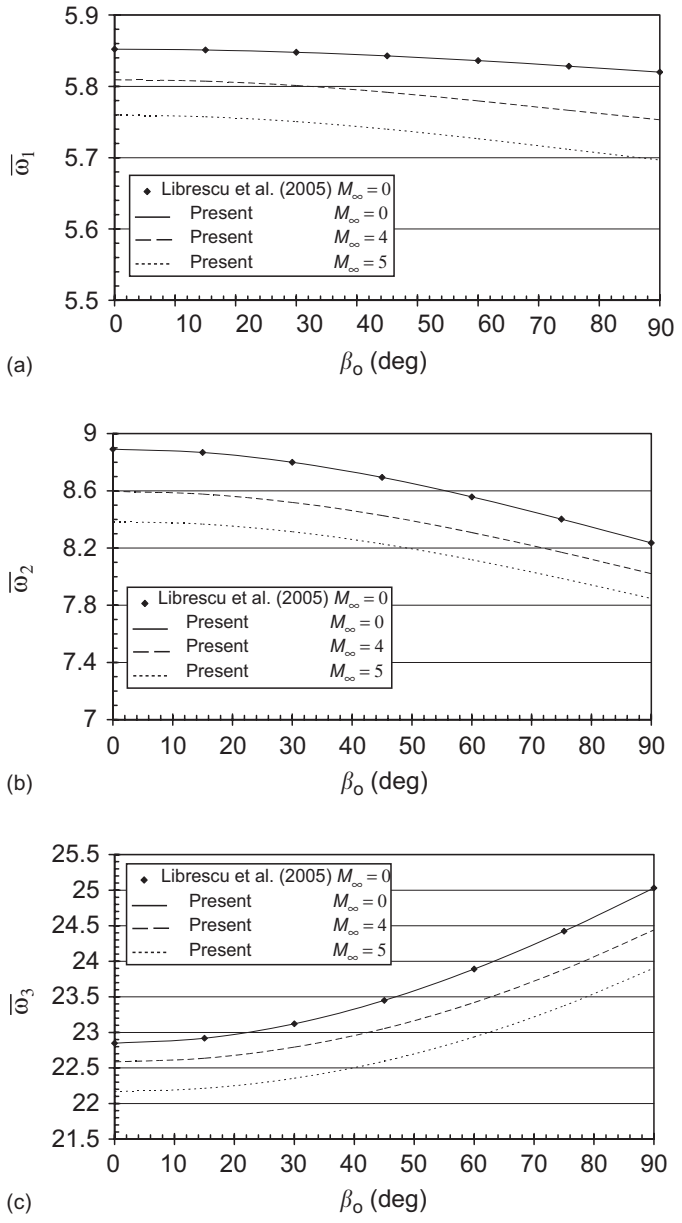

Fig. 4. Variation of the natural frequencies versus pre-twist angle for selected values of Mach number for $\bar{\Omega} = 3$, $\gamma = 0$, and $k = 0$.

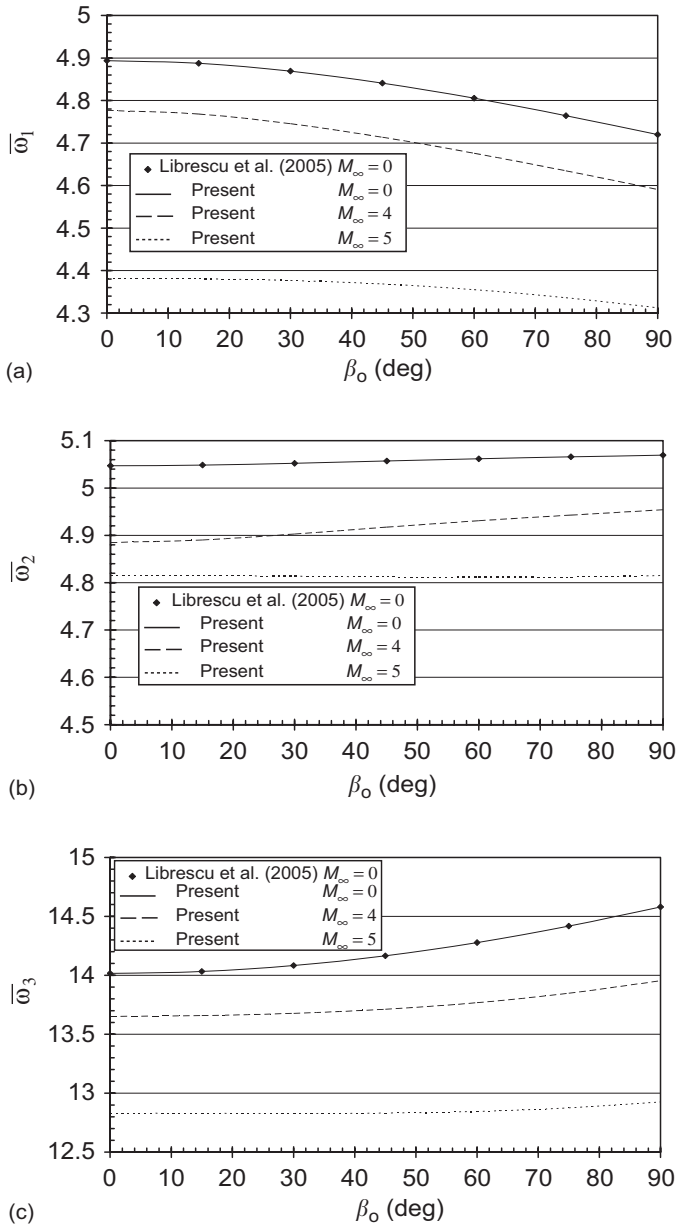

Fig. 5. Variation of the natural frequencies versus pre-twist angle for selected values of Mach number for $\bar{\Omega} = 3$, $\gamma = 0$, and $k = 50$.

In Fig. 4 the influence of pre-twist angle with associated Mach number is investigated. An increasing Mach number has similar effects as discussed for previous figures. In Fig. 5 the results for a full metal blade are presented. Fig. 6 shows the variation of natural frequencies versus the volume fraction parameter. It is evident from these plots that increasing the Mach number and the volume fraction parameter influences strongly the natural frequencies. These results are consistent with those presented in the previous plots.

8. Conclusion

The behavior of rotating beams made up of functionally graded materials exposed to high-temperature supersonic gas flow is investigated. The proposed formulation enables one to accurately and efficiently describe blade

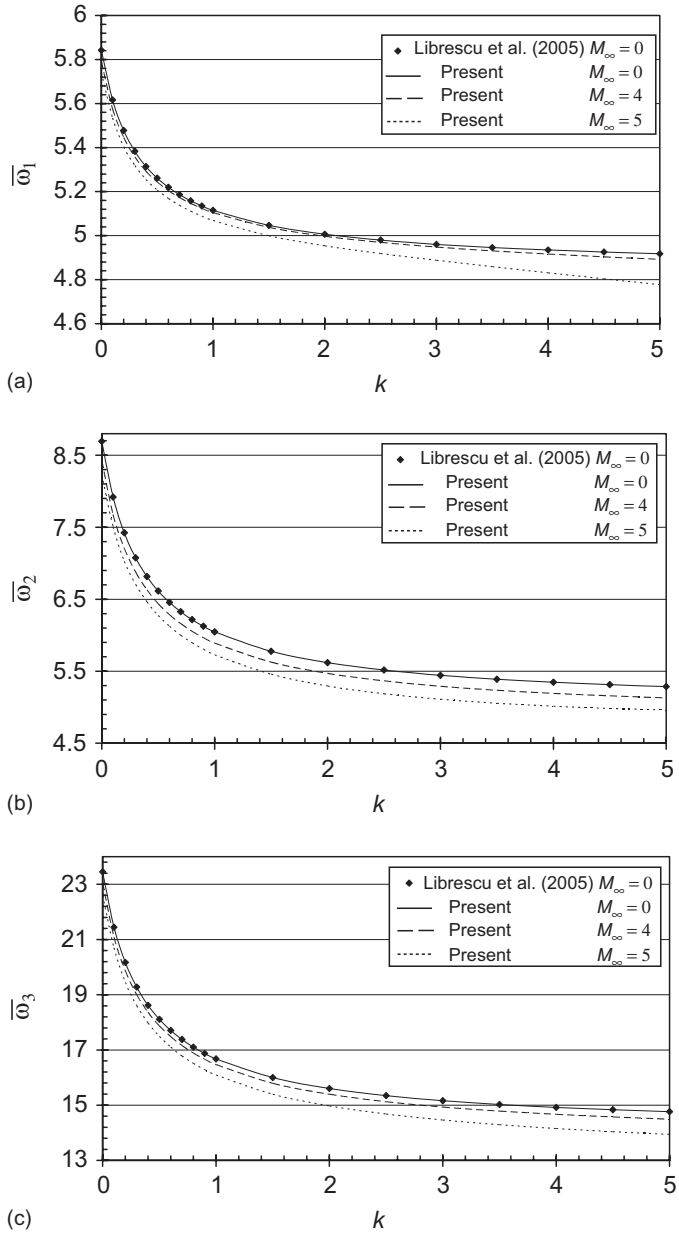

Fig. 6. Variation of the natural frequencies versus volume fraction parameter k for $\beta_0 = 45^\circ$, $\bar{\Omega} = 3$, and $\gamma = 0$.

natural frequencies when it is subjected to actual operating conditions. The effects of the volume fraction index, pre-twist angle, rotating speed, and Mach number on the flutter or natural frequencies have been demonstrated. A reasonable agreement is obtained for zero Mach number between the present solution and those of Librescu et al. (2005).

A detailed parametric study of the proposed model reveals the following points:

(i) with an increase in volume fraction index, the natural frequencies decrease exponentially;
(ii) the natural frequencies increase with increasing rotating speed, and decrease with increasing Mach number;

(iii) the natural frequencies are dependent on the pre-twist angle (β_0) as well as the Mach number;
(iv) the natural frequencies decrease under aerothermoelastic loadings, especially at high Mach numbers.

Appendix A

Expressions for the elements of the mass, aerodynamic damping and stiffness matrices are as follows:

$$[M]=\begin{bmatrix} m_{11} & 0 & 0 & 0 \\ 0 & m_{22} & 0 & 0 \\ 0 & 0 & m_{33} & m_{34} \\ 0 & 0 & m_{43} & m_{44} \end{bmatrix}, \tag{A.1}$$

where

$$m_{11}=\int_0^L b_1\{U\}\{U\}^{\mathrm{T}}\,\mathrm{d}z, \quad m_{22}=\int_0^L b_1\{V\}\{V\}^{\mathrm{T}}\,\mathrm{d}z,$$
$$m_{33}=\int_0^L (b_4+b_{14})\{\Theta_x\}\{\Theta_x\}^{\mathrm{T}}\,\mathrm{d}z, \quad m_{44}=\int_0^L (b_5+b_{15})\{\Theta_y\}\{\Theta_y\}^{\mathrm{T}}\,\mathrm{d}z,$$
$$m_{34}=\int_0^L (b_6-b_{13})\{\Theta_x\}\{\Theta_y\}^{\mathrm{T}}\,\mathrm{d}z, \quad m_{43}=\int_0^L (b_6-b_{13})\{\Theta_y\}\{\Theta_x\}^{\mathrm{T}}\,\mathrm{d}z,$$

$$[G]=\begin{bmatrix} g_{11} & g_{12} & 0 & 0 \\ g_{21} & g_{22} & 0 & 0 \\ 0 & 0 & 0 & 0 \\ 0 & 0 & 0 & 0 \end{bmatrix}, \tag{A.2}$$

where

$$g_{11}=\int_0^L (-aS_{\beta\gamma}^2-bC_{\beta\gamma}^2)C_\infty\rho_\infty\{U\}\{U\}^{\mathrm{T}}\,\mathrm{d}z, \quad g_{12}=\int_0^L (a-b)C_\infty\rho_\infty C_{\beta\gamma}S_{\beta\gamma}\{U\}\{V\}^{\mathrm{T}}\,\mathrm{d}z,$$
$$g_{21}=\int_0^L (a-b)C_\infty\rho_\infty C_{\beta\gamma}S_{\beta\gamma}\{V\}\{U\}^{\mathrm{T}}\,\mathrm{d}z, \quad g_{22}=\int_0^L (-aC_{\beta\gamma}^2-bS_{\beta\gamma}^2)C_\infty\rho_\infty\{V\}\{V\}^{\mathrm{T}}\,\mathrm{d}z,$$

$$[K]=\begin{bmatrix} k_{11} & k_{12} & k_{13} & k_{14} \\ k_{21} & k_{22} & k_{23} & k_{24} \\ k_{31} & k_{32} & k_{33} & k_{34} \\ k_{41} & k_{42} & k_{43} & k_{44} \end{bmatrix},$$

where

$$k_{11}=\int_0^L (a_{44}\{U\}'\{U\}'^{\mathrm{T}}-b_1\Omega^2\{U\}\{U\}^{\mathrm{T}}+\Omega^2R\{U\}'\{U\}'^{\mathrm{T}}+(-aU_{y^p}^tS_{\beta\gamma}^2-bU_{x^p}^tC_{\beta\gamma}^2)C_\infty\rho_\infty\{U\}\{U\}^{\mathrm{T}})\,\mathrm{d}z,$$

$$k_{12}=\int_0^L (a_{45}\{U\}'\{V\}'^{\mathrm{T}}+(aU_{y^p}^t-bU_{x^p}^t)C_\infty\rho_\infty C_{\beta\gamma}S_{\beta\gamma}\{U\}\{V\}'^{\mathrm{T}})\,\mathrm{d}z,$$

$$k_{13}=\int_0^L (a_{45}\{U\}'\{\Theta_x\}^{\mathrm{T}})\,\mathrm{d}z, \quad k_{14}=\int_0^L (a_{44}\{U\}'\{\Theta_y\}^{\mathrm{T}})\,\mathrm{d}z,$$

$$k_{21}=\int_0^L (a_{45}\{V\}'\{U\}'^{\mathrm{T}}+(aU_{y^p}^t-bU_{x^p}^t)C_\infty\rho_\infty C_{\beta\gamma}S_{\beta\gamma}\{V\}\{U\}'^{\mathrm{T}})\,\mathrm{d}z,$$

$$k_{22}=\int_0^L (a_{55}\{V\}'\{V\}'^{\mathrm{T}}+\Omega^2R\{V\}'\{V\}'^{\mathrm{T}}+(-aU_{y^p}^tC_{\beta\gamma}^2-bU_{x^p}^tS_{\beta\gamma}^2)C_\infty\rho_\infty\{V\}\{V\}'^{\mathrm{T}})\,\mathrm{d}z,$$

$$k_{23}=\int_0^L (a_{55}\{V\}'\{\Theta_x\}^{\mathrm{T}})\,\mathrm{d}z,\quad k_{24}=\int_0^L (a_{45}\{V\}'\{\Theta_y\}^{\mathrm{T}})\,\mathrm{d}z,$$

$$k_{31}=\int_0^L (a_{45}\{\Theta_x\}\{U\}'^{\mathrm{T}})\,\mathrm{d}z,\quad k_{32}=\int_0^L (a_{55}\{\Theta_x\}\{V\}'^{\mathrm{T}})\,\mathrm{d}z,$$

$$k_{33}=\int_0^L (a_{55}\{\Theta_x\}\{\Theta_x\}^{\mathrm{T}}-(b_4+b_{14})\Omega^2\{\Theta_x\}\{\Theta_x\}^{\mathrm{T}}+a_{33}\{\Theta_x\}'\{\Theta_x\}'^{\mathrm{T}})\,\mathrm{d}z,$$

$$k_{34}=\int_0^L (a_{45}\{\Theta_x\}\{\Theta_y\}^{\mathrm{T}}-(b_6-b_{13})\Omega^2\{\Theta_x\}\{\Theta_y\}^{\mathrm{T}}+a_{23}\{\Theta_x\}'\{\Theta_y\}'^{\mathrm{T}})\,\mathrm{d}z,$$

$$k_{41}=\int_0^L (a_{44}\{\Theta_y\}\{U\}'^{\mathrm{T}})\,\mathrm{d}z,\quad k_{42}=\int_0^L (a_{45}\{\Theta_y\}V'^{\mathrm{T}})\,\mathrm{d}z,$$

$$k_{43}=\int_0^L (a_{45}\{\Theta_y\}\{\Theta_x\}^{\mathrm{T}}-(b_6-b_{13})\Omega^2\{\Theta_y\}\{\Theta_x\}^{\mathrm{T}}+a_{23}\{\Theta_y\}'\{\Theta_x\}'^{\mathrm{T}})\,\mathrm{d}z,$$

$$k_{44}=\int_0^L (a_{44}\{\Theta_y\}\{\Theta_y\}^{\mathrm{T}}-(b_5+b_{15})\Omega^2\{\Theta_y\}\{\Theta_y\}^{\mathrm{T}}+a_{22}\{\Theta_y\}'\{\Theta_y\}'^{\mathrm{T}})\,\mathrm{d}z.$$

References

Aboudi, J., Pindera, M., Arnold, S.M., 1996. Thermoelastic theory for response of materials functionally graded in two directions. International Journal of Solids and Structures 33, 931–966.

Aboudi, J., Pindera, M., Arnold, S.M., 1999. Higher-order theory for functionally graded materials. Composites: Part B 30, 777–832.

Chandiramani, N.K., Shete, Ch.D., Librescu, L., 2003. Vibration of higher-order-shearable pretwisted rotating composite blades. International Journal of Mechanical Sciences 45, 2017–2041.

Dowell, E.H., 1975. Aeroelasticity of Plates and Shells. Noordhoff International Publishing, Leyden, Netherlands.

Lanhe, Wu., 2004. Thermal buckling of a simply supported moderately thick rectangular FGM plate. Composite Structures 64, 211–218.

Librescu, L., 1975. Elastostatics and Kinetics of Anisotropic and Heterogeneous Shell-type Structures. Noordhoff International Publishing, Leyden, Netherlands.

Librescu, L., Oh, S.Y., Song, O., 2005. Thin-walled beams made of functionally graded materials and operating in a high temperature environment: vibration and instability. Journal of Thermal Stresses 28, 694–712.

Noda, N., Hetnarski, R.B., Tanigawa, Y., 2003. Thermal Stresses, second ed. Taylor & Francis, New York.

Oh, S.Y., Librescu, L., Song, O., 2003a. Thermoelastic modeling and vibration of functionally graded thin-walled rotating blades. AIAA Journal 41, 2051–2060.

Oh, S.Y., Librescu, L., Song, O., 2003b. Vibration of turbomachinery rotating blades made of functionary graded materials and operating in a high temperature field. Acta Mechanica 166, 69–87.

Pindera, M.J., Aboudi, J., Arnold, S.M., 1995. Limitations of the uncoupled, RVE-based micromechanical approach in the analysis of functionally graded composites. Mechanics of Materials 20, 77–94.

Pourtakdoust, S.H., Fazelzadeh, S.A., 2005. Nonlinear aerothermoelastic behavior of skin panel with wall shear stress effect. Journal of Thermal Stresses 28, 147–169.

Praveen, G.N., Reddy, J.N., 1998. Nonlinear transient thermoelastic analysis of functionally graded ceramic metal plates. International Journal of Solids and Structures 35, 4457–4476.

Qin, Z., Librescu, L., 2002. On a shear-deformed theory of anisotropic thin-walled beams: further contribution and validations. Composite Structures 56, 345–358.

Reddy, J.N., 1986. Applied Functional Analysis and Variational Methods in Engineering, second ed. McGraw-Hill, New York.

Reddy, J.N., Chin, C.D., 1998. Thermomechanical analysis of functionally graded cylinders and plates. Journal of Thermal Stresses 21, 593–626.

Sanker, B.V., Tzeng, T.J., 2002. Thermal stresses in functionally graded beams. AIAA Journal 40, 1228–1232.